

CoDeGAN: Contrastive Disentanglement for Generative Adversarial Network

Jiangwei Zhao^a, Zejia Liu^a, Xiaohan Guo^a, Lili Pan^{a,*}

^a School of Information and Communication Engineering, University of Electronic Science and Technology of China, Chengdu, 611731, China

Abstract

Disentanglement, a critical concern in interpretable machine learning, has also garnered significant attention from the computer vision community. Many existing GAN-based class disentanglement (unsupervised) approaches, such as InfoGAN and its variants, primarily aim to maximize the mutual information (MI) between the generated image and its latent codes. However, this focus may lead to a tendency for the network to generate highly similar images when presented with the same latent class factor, potentially resulting in mode collapse or mode dropping. To alleviate this problem, we propose CoDeGAN (Contrastive Disentanglement for Generative Adversarial Networks), where we relax similarity constraints for disentanglement from the image domain to the feature domain. This modification not only enhances the stability of GAN training but also improves their disentangling capabilities. Moreover, we integrate self-supervised pre-training into CoDeGAN to learn semantic representations, significantly facilitating unsupervised disentanglement. Extensive experimental results demonstrate the superiority of our method over state-of-the-art approaches across multiple benchmarks. The code is available at <https://github.com/learninginvision/CoDeGAN>.

Keywords: Generative adversarial networks, disentanglement, image generation, pre-training methods

1. Introduction

Considerable efforts have been dedicated to enhancing interpretable and controllable generation (Doshi-Velez and Kim, 2017; Lakkaraju et al., 2016; Rudin, 2019; Zhang et al., 2018) through constructing controllable deep generative models. Notably, several models have been successfully proposed, including InfoGAN (Chen et al., 2016) and its variants (Lin et al., 2020; Ojha et al., 2020; Mukherjee et al., 2019), Factor-VAE (Kim and Mnih, 2018), and β -VAE (Higgins et al., 2016). Within these endeavors, representation disentanglement (Gabbay and Hoshen, 2020; Liu et al., 2020; Locatello et al., 2020; Shu et al., 2020) has garnered significant attention.

Representation disentanglement refers to the problem of learning a representation that can separate the distinct and informative factors of variations in data. In recent years, the majority of literature concerning disentanglement (Kingma and Welling, 2014; Higgins et al., 2016; Gabbay and Hoshen, 2020; Liu et al., 2020; Locatello et al., 2020; Shu et al., 2020; Kim and Mnih, 2018; Chen et al., 2016; Kim and Ha, 2021; Hwang et al., 2021) has concentrated on Bayesian generative models like VAE (Kingma and Welling, 2014), β -VAE (Higgins et al., 2016), and Factor-VAE (Kim and Mnih, 2018). These models allow for the learning of representation through latent variable models with some structure prior. In contrast, scant attention (Chen et al., 2016; Kim and Ha, 2021; Hwang et al., 2021) has been devoted to GAN-based disentanglement, although GANs have a remarkable ability in generation compared to VAE. We suspect this discrepancy arises from the inherent difficulty of posterior inference in GANs, which has posed

a significant challenge to GAN-based disentanglement (Mohamed and Lakshminarayanan, 2016; Pan et al., 2020).

Maximizing mutual information (MI) (Chen et al., 2016) is one of the few choices in the GANs family that can produce disentangled representations. Thus, InfoGAN and its variants have been widely used in multi-factor (*i.e.*, background, object, and texture) disentanglement to facilitate conditional image generation (Kim and Ha, 2021; Benny and Wolf, 2020; Li et al., 2020). Despite their wide usage in real-world applications, no previous study shows they may inherently incur the instability of GAN's training, and deteriorate disentanglement performance. In InfoGAN, MI is defined as the mutual information between the generated image and the latent code. Specifically, if c denotes the latent code and \mathbf{z} denotes in-compressible noise, the MI term is defined as:

$$I(G(\mathbf{z}, c); c) = H[G(\mathbf{z}, c)] - H[G(\mathbf{z}, c)|c], \quad (1)$$

where $H(\cdot)$ denotes entropy and $G(\mathbf{z}, c)$ denotes the synthesised image. Maximizing Eq. (1) may significantly limit diversity, especially when c is discrete, as it maximizes the reduction in uncertainty about $G(\mathbf{z}, c)$ under being told the value of c . This may incur the instability of GAN's training, potentially leading to mode collapse or mode dropping. Although in InfoGAN, the actual loss is the variational lower bound on the mutual information, it enforces that images generated with the same latent code c can be encoded to c . Such a loss would also reduce generative diversity dramatically, hindering generative distribution from getting close to real distribution. To alleviate this problem, especially in discrete factor disentanglement (*i.e.*, class disentanglement), we propose contrastive disentanglement in GANs, where we relax the similarity constraint to the feature domain, rather than the input image domain.

*Corresponding author.

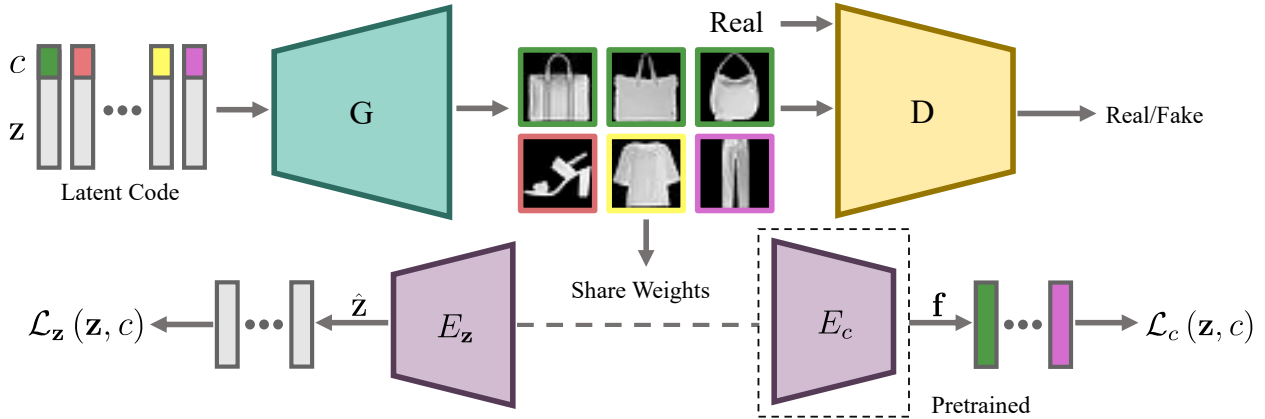


Figure 1: **Contrastive disentanglement framework.** The input of generator G consists of two parts: (i) $c \sim \text{mul}(\pi)$, which controls the detailed class and (ii) $z \sim \mathcal{N}(\mathbf{0}, \sigma^2 \mathbf{I})$, which corresponds to intra-class variation. The representation f encoded by E_c is regularized by contrastive loss \mathcal{L}_c for disentanglement, while the representation \hat{z} encoded by E_z is regularized by reconstruction loss \mathcal{L}_z for preserving intra-class variation. E_c and E_z could share weights partly. The definitions of positive and negative pairs in \mathcal{L}_c are images within the same class or not.

Another problem in maximizing MI-based GAN disentanglement approaches is that they learn image generation and latent factor disentanglement jointly. Without any guidance, they have difficulty in learning univocal latent factors. As of now, such a problem almost remains unexplored. Inspired by the rapid development of self-supervised pre-training methods (Chen et al., 2020; He et al., 2020; Wu et al., 2018; Jaiswal et al., 2021) in recent years, we recognize that pre-training may facilitate learning semantically meaningful representations for unsupervised disentanglement. To this end, we integrate self-supervised pre-training into our contrastive disentanglement framework, striving to enforce the encoder to learn semantic representation in disentanglement. As illustrated in Fig. 1, the encoder for extracting class-related features can be pre-trained.

To sum up, this work shows two inherent problems in GAN-based disentanglement, and to alleviate these two problems, we propose **Contrastive Disentanglement for Generative Adversarial Networks (CoDeGAN)**. On the one hand, the proposed model, by relaxing the similarity constraint, can improve performance in both disentanglement accuracy and generative quality. On the other hand, CoDeGAN can naturally integrate self-supervised pre-training into GAN-based disentanglement, further improving disentanglement accuracy. As shown in Fig. 3, we improve GAN’s training stability, resulting in significantly improved Fréchet Inception Distance (FID) and ACC. On the CIFAR-10 dataset, we gain a stunning 19% absolute improvement over InfoGAN and 16% absolute improvement over the previous SOTA methods. Not only that, we achieve the SOTA performance on other datasets. Our findings will offer some fresh insights into the field of GAN-based disentanglement.

2. Related Work

Our work relates to several research fields. We describe prior work for these broad fields, including disentanglement approaches based on variational autoencoders (VAEs) and gener-

ative adversarial networks (GANs), as well as self-supervised pre-training.

2.1. VAE-based Disentanglement.

VAE-based disentanglement methods (Chen et al., 2018; Higgins et al., 2016; Kim and Mnih, 2018) attempt to learn disentangled representations by encouraging the posterior distribution of latent code to be close to certain prior distributions. β -VAE (Higgins et al., 2016) uses a larger weight on the KL divergence between the variational posterior and the prior to fulfill disentanglement. β -TCVAE (Chen et al., 2018) estimates the total correlation (TC), a measure of the statistical dependence or redundancy among the latent variables, by minibatch-weighted sampling, and places more emphasis on minimizing the TC. This encourages the latent variables to become more independent and disentangled. Factor-VAE (Kim and Mnih, 2018) utilizes a discriminator network to predict latent code to estimate the TC, avoiding the computational complexity of directly calculating high-dimensional TC. Recently, the work (Locatello et al., 2020) has proposed to use few labels to disentangle factors of variation under the VAE framework. These methods have been shown to be capable of disentangling *continuous* factors with some success; however, they are not well-suited to capture *discrete* factors.

In contrast, our research focuses on disentangling *discrete* factors, a direction that has received relatively little attention in VAE-based disentanglement approaches.

2.2. GAN-based Disentanglement.

GANs-based disentanglement methods (Esser et al., 2020; Chen et al., 2016; Lin et al., 2020; Mukherjee et al., 2019; Shen et al., 2020) can be categorized into two classes: unsupervised and supervised. In this work, we mainly focus on unsupervised disentanglement. InfoGAN (Chen et al., 2016), as one typical unsupervised method, maximizes the mutual information between an image and its latent codes. InfoGAN-CR (Lin

et al., 2020), compared to InfoGAN, adds a contrastive regularizer (CR) to encourage paired images with shared factor to be similar. Although InfoGAN-CR uses the concept of contrastive regularization, it does not include the contrastive loss into the model. Elastic-InfoGAN (Ojha et al., 2020) introduces contrastive loss as an auxiliary loss of InfoGAN, and forces the encoder to learn features focusing on image classes to disentangle class-imbalanced data. ClusterGAN (Mukherjee et al., 2019) trains the GANs and the inverse-mapping network under a clustering-specific loss.

Although the idea of contrastive learning has been explored in some of the above disentanglement works (Ren et al., 2021; Kim and Ha, 2021; Hwang et al., 2021), our work is the *first* study that explores removing the MI term and relies only on the contrastive loss for discrete factor disentanglement.

Except for unsupervised discrete factor disentanglement, there exist some other studies for unsupervised continuous factor disentanglement. InterFaceGAN (Esser et al., 2020) proposed an invertible interpretation network to disentangle the representations of semantic concepts. StyleGAN (Karras et al., 2019) has achieved significant success in image generation, and the decoupling of its latent space is an important direction for disentanglement. Analyzing changes in generated images by shifting latent codes enables the identification of relationships between latent codes and attributes of the generated images. GANSpace (Härkönen et al., 2020) uses principal component analysis to decompose the latent space so as to discover image attribute editing directions in StyleGAN. SeFa (Shen and Zhou, 2021) proposes a closed-form factorization algorithm for latent semantic factor discovery. SRE (Kappiyath et al., 2022) proposes a scale ranking estimator, which distinguishes and captures the most important factors of variation by ranking the magnitude of variation of the latent code in the generated image along each direction. DisCo (Ren et al., 2021) proposed a model-agnostic method to disentangle continuous factors, where a navigator is trained with the contrastive loss to provide disentanglement directions. It distinctly differs from our work as it is for continuous factor disentanglement.

In contrast to previous unsupervised disentanglement works, our method has three obvious differences: (i) it has no MI term, (ii) it only relies on the contrastive loss for discrete factor disentanglement, and (iii) it leverages pre-training to extract semantically meaningful features to facilitate disentanglement.

2.3. Self-supervised pre-training.

Self-supervised pre-training is a form of unsupervised training that captures the intrinsic patterns and properties of data without using human-provided labels to learn discriminative representations for downstream tasks (Sohn, 2016; Chen et al., 2020; He et al., 2020; Wu et al., 2018; Khosla et al., 2020; Oord et al., 2018; Wang et al., 2021; Caron et al., 2020; He et al., 2022). In computer vision, SimCLR first establishes a general framework for self-supervised pre-training using a contrastive scheme (Chen et al., 2020). Momentum Contrast (MoCo) (He et al., 2020; Wu et al., 2018) further demonstrates the effect of increasing negative pairs on promoting contrastive learning (CL) performance. Later, SimSiam (Chen and He,

2021) has shown that stop-gradient operation plays an essential role in preventing collapse solutions, and even not using negative sample pairs, large batches and momentum encoders can learn meaningful representations. Meanwhile, some theoretical papers (Arora et al., 2019; Oord et al., 2018; Tschanen et al., 2019; Wang and Isola, 2020; Wu et al., 2020; Hjelm et al., 2018) discuss the relationship between contrastive self-supervised learning and the InfoMax principle, and interpret the success of CL from this perspective. With the success of vision transformer (ViT), DINO (Caron et al., 2021), which trains a ViT in a self-supervised manner, further bridges the gap between self-supervised pre-training and ViT. MAE (He et al., 2022) adopts masked image modeling (MIM) in self-supervised pre-training, which uses an asymmetric encoder-decoder to reconstruct the masked input image patches, and achieves improved performance in downstream tasks. CLIP (Radford et al., 2021) pre-trains one textual encoder and one image encoder for text-image alignment on a large-scale text-image dataset. BLIP (Li et al., 2022) is a new VLP framework that enables a wider range of downstream tasks. It introduces a multi-modal mixture of Encoder-Decoder structure for unified vision-language understanding and generation, which can effectively perform multi-task pre-training and transfer learning.

In this work, we hope to explore how self-supervised pre-training can facilitate representation disentanglement.

3. Contrastive Disentanglement in GANs

3.1. Contrastive Disentanglement Framework

Generative adversarial networks (GANs), as a fundamental deep generative model, directly learn a generator G mapping from input latent variables \mathbf{z} to image, and a discriminator D to discriminate real and fake images. Specifically, it trains D to maximize the probability of correct discriminating between real and generative images and simultaneously trains G to maximize the probability of the generated image being recognized as real ones. The objective function is typically formulated as follows:

$$\min_G \max_D \mathbb{E}_{\mathbf{x} \sim p_{data}(\mathbf{x})} [\log D(\mathbf{x})] + \mathbb{E}_{\mathbf{z} \sim p(\mathbf{z})} [\log (1 - D(G(\mathbf{z})))] . \quad (2)$$

Here, $D(\mathbf{x})$ represents the probability of \mathbf{x} being real, while $D(G(\mathbf{z}))$ pertains to the generated image $G(\mathbf{z})$.

The task of disentanglement in GANs presents a challenge, as it is difficult to formulate a latent variable model with a data structure prior. In order to overcome this obstacle, we propose to disentangle the class variation of data by comparing the features of generated images. Our approach is based on the idea that the same factor will create similar image features that are associated with the factor.

To disentangle the class variation, which is the commonest in visual data, we define the input latent code consists of two parts: (i) $c \sim \text{mul}(\boldsymbol{\pi})$, which controls the detailed class and (ii) $\mathbf{z} \sim \mathcal{N}(\mathbf{0}, \sigma^2 \mathbf{I})$, which corresponds to intra-class variation. Then, for each generated image $G(\mathbf{z}, c)$, given the discriminator

D , the loss for generator now change to be:

$$\mathcal{L}_{GAN} = \mathbb{E}_{\mathbf{z}, c \sim p(\mathbf{z}, c)} [\log(1 - D(G(\mathbf{z}, c)))] \quad (3)$$

where $p(\mathbf{z}, c)$ can be rewritten as $p(\mathbf{z})p(c)$ as \mathbf{z} and c are independent variables.

Inspired by the intuition that the same latent class variable should produce images in the same class, we use an encoder to extract representation \mathbf{f} , *i.e.*, $\mathbf{f} = E_c(G(\mathbf{z}, c))$ and construct contrastive loss \mathcal{L}_c for feature \mathbf{f} . We hope the same c , even combined with different \mathbf{z} , produces similar features \mathbf{f} , and vice versa. Let $p_{pos}(\cdot, \cdot)$ be the positive distribution about (\mathbf{z}, c) over $\mathbb{R}^{D+1} \times \mathbb{R}^{D+1}$, $p(\mathbf{z}, \text{neg}(c))$ be the distribution of negative samples. Here, $\text{neg}(c) \sim \text{mul}(\boldsymbol{\pi})$, $\pi_k = 1/K$, $\text{neg}(c) \neq c$. By comparing positive and negative pairs, we formulate $\mathcal{L}_c(\mathbf{z}, c)$ as:

$$\mathbb{E}_{\substack{(\mathbf{z}, c, \mathbf{z}^+, c^+) \sim p_{pos} \\ (\mathbf{z}_i, c_i^-) \stackrel{i.i.d.}{\sim} p(\mathbf{z}, \text{neg}(c))}} \left[-\log \frac{e^{(\mathbf{f}^T \mathbf{f}^+ / \tau)}}{e^{(\mathbf{f}^T \mathbf{f}^+ / \tau)} + \sum_i e^{(\mathbf{f}^T \mathbf{f}_i^- / \tau)}} \right] \quad (4)$$

where $\tau > 0$ is a scalar temperature hyper-parameter. Here, \mathbf{f}^+ is the feature from positive samples, *i.e.*, $E_c(G(\mathbf{z}^+, c^+))$, $c^+ = c$, \mathbf{z}^+ is a sampling point from $p(\mathbf{z})$ and $\mathbf{z} \neq \mathbf{z}^+$. Each (\mathbf{z}, c) has one positive pair and $K - 1$ negative pairs. Similarly, \mathbf{f}_i^- is the feature from negative samples, *i.e.*, $E_c(G(\mathbf{z}_i, c_i^-))$, $c_i^- \neq c$. Eq. (4) encourages the generated images with the same latent code c to have similar features \mathbf{f} , and the images with different latent code c have unlike \mathbf{f} , as shown in Fig. 1. Through such a contrastive loss, we can formulate the correlation between the class of generative images and latent code c .

Except enforcing the features associated with the class to be similar, we also expect the encoded representation $\hat{\mathbf{z}} = E_z(G(\mathbf{z}, c))$ to preserve intra-class variation (Mukherjee et al., 2019) of data. Here, E_z is the encoder responsible for extracting class-unrelated content. Hence, we formulate a reconstruction loss $\mathcal{L}_z(\mathbf{z}, c)$ between the latent variables \mathbf{z} and representation $\hat{\mathbf{z}}$,

$$\mathcal{L}_z(\mathbf{z}, c) = \mathbb{E}_{(\mathbf{z}, c) \sim p(\mathbf{z}, c)} \|\mathbf{z} - \hat{\mathbf{z}}\|_2^2 \quad (5)$$

The smaller \mathcal{L}_z is, the better the noise \mathbf{z} has been preserved. The reconstruction loss \mathcal{L}_z enforces the representations to be separate, obeying underlying Gaussian distribution, and thus has the potential to prevent mode collapse/dropping.

Finally, the objective function \mathcal{L}_G takes account into the image reality loss \mathcal{L}_{GAN} , the contrastive loss \mathcal{L}_c and the reconstruction loss \mathcal{L}_z :

$$\mathcal{L}_G = \mathbb{E}_{\mathbf{z}, c \sim p(\mathbf{z}, c)} [\log(1 - D(G(\mathbf{z}, c)))] + \beta_1 \mathcal{L}_c(\mathbf{z}, c) + \beta_2 \mathcal{L}_z(\mathbf{z}, c) \quad (6)$$

where β_1 and β_2 are two trade-offs. To constrain the flexibility, we prefer to learn G and $E = \{E_c, E_z\}$ separately. The learning procedure of CoDeGAN is a three-step alternative optimization procedure: (i) update discriminator D , (ii) update generator G , and (iii) update encoder E .

We acknowledge the lower bound on mutual information $I(G(\mathbf{z}, c); c)$ in InfoGAN is indeed a cross-entropy loss between the real class distribution and posterior distribution

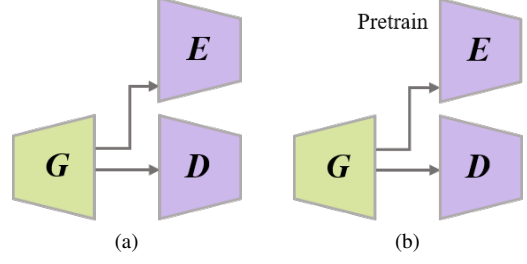


Figure 2: **Comparison of several extensions of the original CoDeGAN.** (a): CoDeGAN. (b): CoDeGAN (self) or CoDeGAN (meta). E_c is pretrained by contrastive learning or meta-learning.

$Q(c|G(\mathbf{z}, c))$. Such a loss enforces similarity among generated images within an exceedingly low-dimensional feature space, potentially diminishing generative diversity. As we discussed previously, diminishing the generative diversity may incur the instability of GAN’s training, resulting in deteriorated disentanglement accuracy.

The reconstruction loss in CoDeGAN, as defined in Eq. (5), bears some resemblance to the previously mentioned cross-entropy loss, as both aim to ensure proximity between the encoded features and the input latent variables. However, owing to the significantly higher dimensionality of the intra-class variables \mathbf{z} and their distinctiveness across each sampling, the reconstruction loss imposed on \mathbf{z} does not diminish diversity but rather encourages it.

3.2. Theoretical Insights

To analyze the contrastive disentanglement loss, we analyze the lower bound of $\mathcal{L}_c(\mathbf{z}, c)$.

Lemma 1. *Minimizing the contrastive loss \mathcal{L}_c is equivalent to maximizing the mutual information between generative representations \mathbf{f} and \mathbf{f}^+ , *i.e.*, $E_c(G(\mathbf{z}, c))$ and $E_c(G(\mathbf{z}^+, c^+))$.*

$$\mathbb{E}_{\substack{(\mathbf{z}, c, \mathbf{z}^+, c^+) \sim p_{pos} \\ (\mathbf{z}_i, c_i^-) \stackrel{i.i.d.}{\sim} p(\mathbf{z}, \text{neg}(c))}} \left[-\log \frac{e^{(\mathbf{f}^T \mathbf{f}^+ / \tau)}}{e^{(\mathbf{f}^T \mathbf{f}^+ / \tau)} + \sum_i e^{(\mathbf{f}^T \mathbf{f}_i^- / \tau)}} \right] \geq \log(K) - I(\mathbf{f}, \mathbf{f}^+) \quad (7)$$

This lower bound indicates that the contrastive disentanglement loss is dominated by the mutual information between \mathbf{f} and \mathbf{f}^+ , which makes intuitive sense and further reveals contrastive disentanglement relax similarity constrains to be in feature domain rather than in image domain.

4. Pre-Training Class Related Encoder

In CL (Tschannen et al., 2019; Arora et al., 2019), the learned representation is always helpful for downstream tasks. In (Arora et al., 2019), the authors demonstrated that the unsupervised loss function $L_{un}(f)$ for contrastive learning could be a surrogate for the downstream supervised tasks,

$$L_{sup}(f) \leq \alpha L_{un}(f), \forall f \in \mathcal{F} \quad (8)$$

where f denotes the representation function, $L_{sup}(f)$ denotes the downstream supervised loss (*i.e.* average classification loss). Here $\alpha \rightarrow 1$ when the number of the latent class is infinite, and the classes occur uniformly in the unlabeled data. This formulation tells us that the representation learned by contrastive learning is semantic. Intuitively, the learned semantic representation can enforce the network to learn meaningful factors. It means contrastive pre-training (which can be unsupervised or supervised) can learn prior knowledge as guidance for disentanglement.

5. Experimental Results

We conduct extensive experiments to assess the effectiveness of our proposed method on widely-used datasets. In the subsequent section, we present the disentanglement accuracy and generative quality of CoDeGAN alongside other baseline approaches.

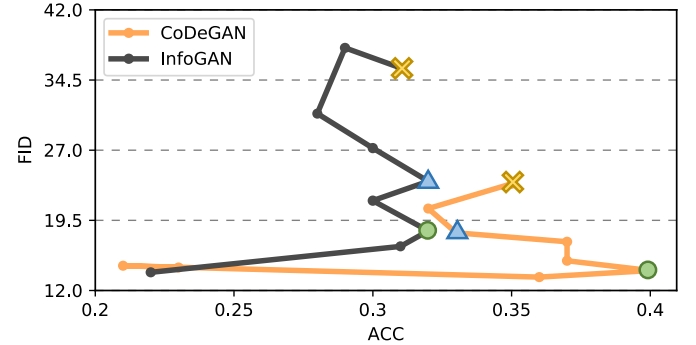
5.1. Experimental Setup

Datasets. The MNIST (Lecun et al., 2001), Fashion-MNIST (Lecun et al., 2001), CIFAR-10 (Krizhevsky et al., 2009), COIL-20 (Nene et al., 1996), 3D-Cars (Fidler et al., 2012), and 3D-Chairs (Aubry et al., 2014) datasets have been widely and consistently used in disentanglement, and they have greatly facilitated progress in the community. The details of these datasets are given below: (i) MNIST (Lecun et al., 2001) has 70,000 28×28 grayscale images of digits ranging from 0 to 9. (ii) Fashion-MNIST (Xiao et al., 2017) has 70,000 images with the size 28×28 . (iii) CIFAR-10 (Krizhevsky et al., 2009) has 60,000 labeled 32×32 RGB natural images in 10 classes. (iv) 3D-Cars (Fidler et al., 2012). It consists of 183 categories, and each category has 96 images. We followed (Ojha et al., 2020) to randomly sample 10 categories (960 RGB images) images, and all images were resized to 64×64 . (v) 3D-Chairs (Aubry et al., 2014). It consists of 1396 total categories, and each category has 62 images with varying positions. We followed (Ojha et al., 2020) to randomly sample 10 categories (620 RGB images) images, and all images were resized to 64×64 . (vi) COIL-20 (Nene et al., 1996). It has 1440 natural images in 20 classes. Following (Mukherjee et al., 2019), all images were resized to 32×32 .

Evaluation metrics. The two criteria for disentanglement model evaluation are disentanglement accuracy and generative quality. Thus, normalized clustering purity (ACC), normalized mutual information (NMI), and adjusted rank index (ARI) are used to evaluate disentanglement accuracy (Mukherjee et al., 2019). Inception Score (IS) (Salimans et al., 2016) and Fréchet Inception Distance (FID) (Heusel et al., 2017) are used to evaluate image quality. The details of these metrics are given below: (i) ACC is designed to calculate the percentage of correct clusters in total samples. (ii) NMI tends to evaluate cluster score by measuring the normalized mutual information between real and clustered labels. (iii) ARI is a metric that measures the similarity of the two clusters by evaluating the proportion of the correct clustering in all clustering results. Following the

work (Mukherjee et al., 2019), given test images, k -means algorithm is adopted to cluster encoded representations, and the best ACC, NMI, and ARI are reported from 5 times run. (iv) IS is calculated by using a pre-trained Inception v3 model to predict the class probabilities for each generated image. (v) FID compares the distributions of Inception embeddings of real data distribution and model distribution. In this work, IS is calculated for ten partitions of 50,000 randomly generated images, and FID is calculated for 50,000 images.

Due to space limitations, more implementation details of our experiment are in Appendix B.



(a) Variations in ACC and FID with different β_1



(b) InfoGAN



(c) CoDeGAN

Figure 3: Disentanglement accuracy and generative quality of CoDeGAN and InfoGAN with different trade-offs on CIFAR-10. (a) X-axis denotes ACC (%), and y-axis denotes FID. **Orange line:** CoDeGAN with loss $\mathcal{L}_{GAN} + \beta_1 \mathcal{L}_c$. **Black line:** InfoGAN with loss $\mathcal{L}_{GAN} + \beta_1 \mathcal{L}_{MI}$. CodeGAN achieves higher ACC and lower FID than InfoGAN for most the trade-offs. (b) The worst generated images of CoDeGAN with different trade-offs. (c) The worst generated images of InfoGAN with different trade-offs. From left to right, the generated images corresponds to the best (green circle), the much larger (blue triangle), and the largest (yellow cross) β_1 . The presence of red boxes in (b) and (c) indicates mode collapse for some certain class.

5.2. Disentanglement Performance against Different Trade-offs

To demonstrate CoDeGAN enhances generation performance and disentanglement accuracy, we conduct a comparative analysis between CoDeGAN, employing only the contrastive loss

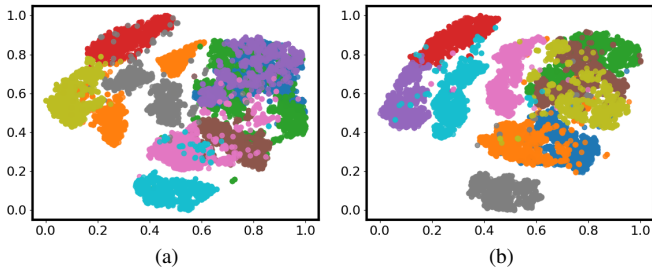


Figure 4: **Visualization of the encoded features of the generated images by variant CoDeGANs.** For all settings, 10000 points are sampled from $p(\mathbf{z}, c)$, the number of sampled points for each fixed c is the same, and different color corresponds to different values of factor c . (a): CoDeGAN. (b): CoDeGAN with pre-trained E_c . The encoder E_c is pre-trained using SimCLR.

$\mathcal{L}_c(\mathbf{z}, c)$, and InfoGAN. Our comparison encompasses disentanglement accuracy and generation quality. Specifically, we evaluate the ACC and FID values of CoDeGAN and InfoGAN across various trade-offs. Fig. 3a illustrates the ACC and FID curves on CIFAR-10. Fig. 3b and Fig. 3c illustrate the worst image generated by InfoGAN and CoDeGAN.

It is apparent that increasing β_1 in CoDeGAN worsens FID slowly, while increasing β_1 in InfoGAN decreases FID dramatically. This demonstrates that the contrastive loss, due to alleviating GAN’s training instability, would not dramatically destroy generative quality even when increasing β_1 , thus could leave more room to constrain similarity. One could observe that CoDeGAN is located in the lower right corner of the figure, which means better performance.

To visualize the generation performance of InfoGAN and CoDeGAN with different β_1 , we display their generated images in Fig. 3b and Fig. 3c. Each row corresponds to the best, the larger, and the largest β_1 values. In addition, the worst cases are chosen for display. We observe CoDeGAN has better disentangling results and generation quality compared to InfoGAN. When β_1 is slightly increased, InfoGAN experiences mode collapse while CoDeGAN maintains stable generation. When β_1 is significantly increased, InfoGAN suffers from mode collapse across all classes and exhibits poor generatoin quality while CoDeGAN only experiences mild mode collapse.

5.3. Disentanglement Performance with Pre-Training

Effects of pre-training. To validate the effectiveness of self-supervised pre-training in disentanglement, we compare CoDeGAN with and without pre-trained encoder on Fashion MNIST. Fig. 4 demonstrates that pre-training can learn valid priors as guidance for unsupervised disentanglement. In Fig. 4a, the ‘green’, ‘pink’, and ‘purple’ points in the t-SNE plot are tangled, while the ‘gray’ and ‘orange’ points are not in the same clusters. Fig. 4b shows that contrastive pre-training aids to promote disentanglement performance, where points with the same color become more close.

The results in Fig. 5 further support the idea of integrating pre-training into disentanglement. As can be seen from Figs. 5a and 5b, utilizing the pre-training encoder gains improvement by 10% in ACC (0.65 \rightarrow 0.75) on Fashion-MNIST, 9% in ACC

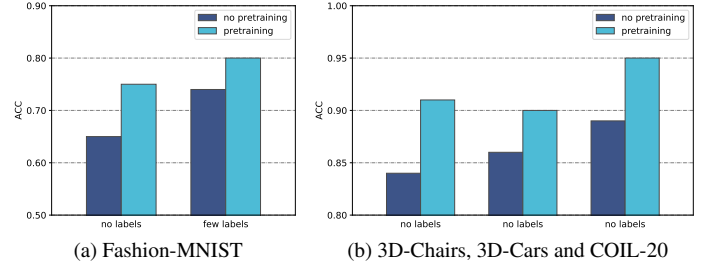


Figure 5: **Disentanglement accuracy of CoDeGAN with and without pre-training.** Pre-training significantly improves the disentanglement accuracy on Fashion-MNIST, 3D-Chairs, 3D-Cars and COIL-20.

(0.84 \rightarrow 0.93) on 3D-Chairs, and 8% in ACC (0.86 \rightarrow 0.94) on 3D-Cars. These are somewhat surprising findings.

In addition, some representative images generated by CoDeGAN, with pre-trained encoder E_c , on 3D-Chairs and 3D-Cars are shown in Fig. 6. Some more results on Fashion-MNIST, COIL-20, and CIFAR-10 are shown in Fig. 7. These results qualitatively confirm that the pre-trained CoDeGAN has the potential to disentangle image variation unsupervisedly.

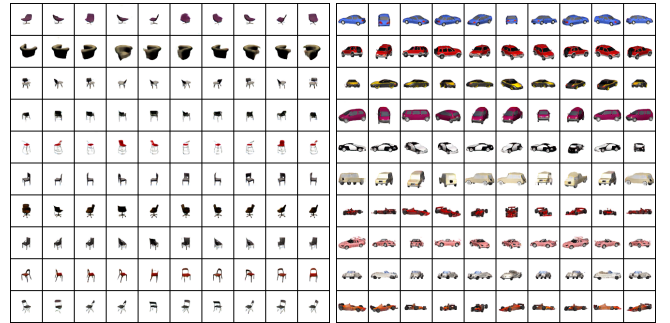


Figure 6: **Example images generated by CoDeGAN for 3D-Chairs and 3D-Cars.** Each row corresponds to one category object with varying pose. The encoder E_c is pre-trained using self-supervised pre-training method—SimCLR.

Pre-training methods study. A potential concern for pre-training is that different pre-training methods could affect the disentanglement accuracy of CoDeGAN. To evaluate this, we compare three recently proposed pre-training methods on the 3D-Chairs, COIL-20, and Fashion-MNIST datasets, including SimCLR (Chen et al., 2020), SimSiam (Chen and He, 2021) and NNCLR (Dwivedi et al., 2021).

Table 1 reports the comparison results. For example, SimCLR’s ACC, NMI and ARI values are 0.91, 0.90, 0.85 on 3D-Chairs, 0.95, 0.95, 0.92 on COIL-20, and 0.75, 0.72, 0.63 on Fashion-MNIST. The reported results reveal the disentanglement accuracy, *i.e.*, ACC, of SimCLR, SimSiam and NNCLR only has slight difference (in 3%, 5%, and 3%) on 3D-Chairs, COIL-20 and Fashion-MNIST. These results suggest that different pre-training methods do not distinctly affect the disentanglement accuracy.

Table 1: **Quantitative comparison of different pre-training methods.** Different pre-training methods do not affect the disentanglement accuracy distinctly.

Datasets	SimCLR (Finn et al., 2017)			SimSiam (Chen et al., 2020)			NNCLR (Dwibedi et al., 2021)		
	ACC↑	NMI↑	ARI↑	ACC↑	NMI↑	ARI↑	ACC↑	NMI↑	ARI↑
3D-Chairs	0.91	0.90	0.85	0.93	0.92	0.89	0.90	0.92	0.87
COIL-20	0.95	0.95	0.92	0.90	0.93	0.86	0.93	0.95	0.90
Fashion-MNIST	0.75	0.72	0.63	0.72	0.67	0.58	0.74	0.69	0.61



Figure 7: **Visualization of the images generated by CoDeGAN (pre-trained) for Fashion-MNIST, COIL-20 and CIFAR-10.**

5.4. Comparison with Baselines

Disentanglement accuracy comparison. To compare with prior work, we conduct testing on Fashion-MNIST, COIL-20, and CIFAR-10. Here, ‘self’ indicates the encoder in CoDeGAN is pre-trained by SimCLR (Chen et al., 2020). The comparison results in Table 2 showcase consistent tendencies. (i) Unsupervised CoDeGAN achieves SOTA performance on multiple benchmarks. On the challenging CIFAR-10 dataset, CoDeGAN gains a stunning 19% absolute improvement over InfoGAN and a 16% absolute improvement over the previous SOTA methods. (ii) Contrastive pre-training can learn prior knowledge to guide disentanglement in unsupervised settings. It gains improvement by 10% in ACC on Fashion-MNIST, and 6% on CIFAR-10, compared to CoDeGAN without pre-training. Considering that SimCLR evaluated using KNN has an accuracy of 0.55 on CIFAR-10 and 0.69 on Fashion-MNIST, it is not surprising that it provides a huge boost to unsupervised disentanglement.

Disentangling category variations of natural images is extremely challenging as these images contain complex backgrounds, object shapes, and appearances. Most unsupervised methods fail on this task, such as disentangling on CIFAR-10. As seen from Table 2, ClusterGAN only has an ACC of 0.18 on CIFAR-10. It is noteworthy that this result is much lower than InfoGAN. A possible explanation for this might be that the encoder of ClusterGAN is separated from the discriminator, leading to learned representations that may not be semantically related to the image category. In contrast, after pre-training, CoDeGAN achieves an ACC of 0.50. The explanations are twofold: (i) The contrastive loss can improve GAN’s equilibrium, leaving more room to constrain disentanglement by in-

creasing the trade-off β_1 . (ii) The pre-trained encoder E_c can guide CoDeGAN to learn semantic representations, enforcing the network to learn meaningful factors.

Generative quality comparison. Table 2 also reports the IS and FID comparison results between our method and other baseline methods on different datasets. For CIFAR-10, our method has the best IS and FID with 8.33 and 13.70 in unsupervised settings, respectively. The results are also significantly better than InfoGAN and InfoGAN-CR. As discussed previously, maximizing MI may limit diversity and break GAN’s equilibrium. In addition, contrastive regularization (CR) may further aggregate mode collapse, as shown in Table 2, where InfoGAN-CR has a FID of 25.19 on CIFAR-10 compared to our result of 14.17.

5.5. Ablation Study

In our ablation study, we analyze the effect of constraining similarity on different feature layers, the effect of the contrastive loss, and the effect of reconstruction loss in CoDeGAN.

Similarity constraint on different feature layer. As mentioned in Section 3.2, contrastive disentanglement relaxes the similarity constraints in the feature domain and is prone to improve GAN’s training stability. To further confirm this, we study the effects of contrastive loss on different feature layers. The features from four layers of the encoder network E_c at different resolutions ($L_1 = 32^2, L_2 = 16^2, L_3 = 8^2, L_4 = 4^2$) were extracted. Here, L_4 denotes the highest feature layer, and L_1 denotes the lowest feature layer, which is the most *close* to the generated image. The features were down-sampled four times

Table 2: **Qualitative comparison with state-of-the-art methods on the Fashion-MNIST, COIL-20 and CIFAR-10 datasets.** *: Trained using open source code.

Algorithm	ACC↑	NMI↑	ARI↑	IS↑	FID↓
<i>Fashion-MNIST</i>					
ClusterGAN (Mukherjee et al., 2019)	0.63	0.64	0.50	-	-
InfoGAN (Chen et al., 2016)	0.61	0.59	0.44	-	-
InfoGAN-CR* (Lin et al., 2020)	0.64	0.64	0.50	4.20	30.35
GAN with bp (Mukherjee et al., 2019)	0.56	0.53	0.37	-	-
GAN with Disc. ϕ (Mukherjee et al., 2019)	0.43	0.37	0.23	-	-
CoDeGAN	0.65	0.66	0.52	4.36	17.09
CoDeGAN (self)	0.75	0.72	0.63	4.18	19.51
<i>COIL-20</i>					
ClusterGAN* (Mukherjee et al., 2019)	0.82	0.89	0.79	4.56	48.13
InfoGAN* (Chen et al., 2016)	0.85	0.90	0.81	4.58	64.49
InfoGAN-CR* (Lin et al., 2020)	0.85	0.90	0.82	4.96	69.71
CoDeGAN	0.89	0.91	0.84	4.54	45.63
CoDeGAN (self)	0.95	0.95	0.92	4.61	46.18
<i>CIFAR-10</i>					
ClusterGAN* (Mukherjee et al., 2019)	0.18	0.05	0.03	8.18	14.95
InfoGAN* (Chen et al., 2016)	0.31	0.21	0.12	7.89	16.71
InfoGAN-CR* (Lin et al., 2020)	0.34	0.24	0.15	7.70	25.19
CoDeGAN	0.44	0.35	0.26	8.29	14.17
CoDeGAN (self)	0.50	0.35	0.27	8.33	13.70

as well as flattened. Then, the multi-scale features were fed to a two-layer MLP, and reduced to the same 128 dimension.

Table 3 shows that CoDeGAN has gradually worse IS and FID when adding contrastive loss \mathcal{L}_c on feature layers that are close to the image. We find the average FID scores for CIFAR-10 and 3D-Chairs fall to 24.27 (15.32 \rightarrow 24.27) and 79.10 (47.08 \rightarrow 79.10), and mode collapse sometimes occurs when adding contrastive loss on lower feature layers. Specifically, after imposing contrastive loss from L_1 to L_4 , the mode collapse rate changes as 0/5 \rightarrow 0/5 \rightarrow 1/5 \rightarrow 4/5 for CIFAR-10. For 3D-Chairs, the collapse rate has advanced: 0/5 \rightarrow 0/5 \rightarrow 1/5 \rightarrow 2/5. These findings suggest that imposing contrastive loss on lower feature layers might adversely affect model stability.

Fig. 8 exhibits some generation results on the 3D-Chair dataset when applying \mathcal{L}_c on different layers. Similar to the observations on CIFAR-10, imposing \mathcal{L}_c on lower layers leads to more obvious mode collapse happens. For generated images where \mathcal{L}_c is applied to $\mathcal{L}_2 + \mathcal{L}_3 + \mathcal{L}_4$, it is observed that the generated images within red boxes, despite having different \mathbf{z} , appear to be identical. When \mathcal{L}_c is imposed to the lowest layer, the frequency of mode collapse escalates. More generated images with mode collapse can be found in Appendix C.3. This tendency may be explained by the fact that the similarity constraints relaxing on low-layer features are slight. This is because these layers are close to the image, and the model capacity of the low-layer sub-networks of the encoder E_c is restricted.

Effect of Contrastive loss. To test the validity of contrastive loss \mathcal{L}_c in terms of disentangling inter-class variation, we set

Table 3: **Disentanglement performance with different features in \mathcal{L}_c .** The results suggest that CoDeGAN has gradually worse IS and FID when adding contrastive loss \mathcal{L}_c on feature layers which are close to image.

Layer				ACC↑	IS↑			FID↓		
L_4	L_3	L_2	L_1	Mean	Max	Mean	Min	Max	Mean	Min
<i>CIFAR-10</i>										
✓				0.39	8.30	8.22	8.10	16.5	15.32	14.11
✓	✓			0.40	8.42	8.11	7.90	16.97	15.86	14.78
✓	✓	✓		0.42	8.32	7.98	7.47	26.62	17.31	12.74
✓	✓	✓	✓	0.43	8.15	7.67	6.86	37.41	24.27	13.92
<i>3D-Chairs</i>										
✓				0.84	3.60	3.45	3.08	77.13	47.08	35.98
✓	✓			0.82	4.03	3.72	3.45	134.40	70.06	37.20
✓	✓	✓		0.79	4.21	3.79	3.57	99.85	72.30	44.39
✓	✓	✓	✓	0.72	3.73	3.40	2.92	119.76	79.10	36.98

the value of β_1 to be zero. Then, the objective function only has two parts: (i) the loss \mathcal{L}_{GAN} , and (ii) the loss \mathcal{L}_z . From the results in Fig. 9a and Fig. 9c, one can observe that there is no disentangling effect on MNIST, even when structured code including content factor \mathbf{z} and class factor c is fed into the network. The ACC score falls to be 0.11 when $\beta_1 = 0$, whereas it rises to 0.98 when $\beta_1 = 75$. Such results soundly demonstrate \mathcal{L}_c can disentangle image category variation.

Effect of reconstruction loss. To study the effect of reconstruction loss \mathcal{L}_z , β_2 is set to be zero. The worst results in 5 time runs are reported. Fig. 9b and Fig. 9d show the mode collapse image at 300 epoch and its corresponding IS and FID scores. Mode collapse occurred two out of five times during the training pro-

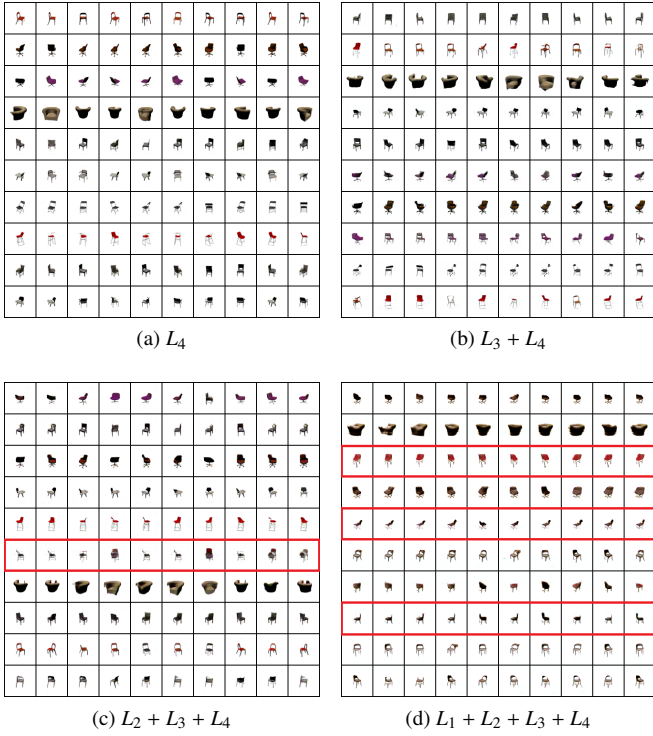


Figure 8: **Visualization of generated images for 3D-Chairs with L_c imposed on the different feature layers.** L_4 denotes the highest feature layer, and L_1 denotes the lowest feature layer, which is most *close* to the input image. Each row is generated with same c and different \mathbf{z} . To facilitate model collapse analysis, we show the worst images from five training times

cess. One can observe that the IS and FID scores fall to 7.56 and 21.97 when the mode collapse happens, while the IS and FID scores are 8.08 and 13.45 when no mode collapse happens. This confirms that the reconstruction loss can further alleviate the mode collapse problem.

6. Conclusion and Future Work

We propose contrastive disentanglement for generative adversarial networks (CoDeGAN) in this paper, with both theoretical analysis and practical algorithmic implementation. After relaxing the similarity constraint to the feature domain, CoDeGAN improves disentanglement accuracy and generation quality. Integrating self-supervised pre-training to learn priors as guidance for disentanglement, CoDeGAN yields further improved disentanglement accuracy. We show that our proposed method achieves the SoTA performance on multiple benchmarks. In this paper, we only consider discrete factor disentanglement since it is harder to consider alleviating GAN’s training instability and pre-training in continuous factor disentanglement. Introducing pre-training techniques to multi-factor (which can be discrete or continuous) disentanglement is still an open problem.



\mathcal{L}_c	ACC \uparrow	NMI \uparrow	ARI \uparrow	\mathcal{L}_z	IS \uparrow	FID \downarrow	ACC \uparrow
W	0.98	0.96	0.96	W	8.08	13.45	0.72
o	0.11	0.00	0.00	o	7.56	21.97	0.69

Figure 9: **Ablation study of contrastive loss \mathcal{L}_c and reconstruction losses \mathcal{L}_z .** (a) disentanglement result without \mathcal{L}_c (b) generation result without \mathcal{L}_z , (c) ACC, NMI and ARI scores with and without \mathcal{L}_c , (d) IS and FID scores with and without \mathcal{L}_z .

Acknowledgment

This work is partially supported by the National Natural Science Foundation of China (No. 62171111) and Natural Science Foundation of Sichuan Province (2023NSFSC1972).

Appendix A. Proofs

Lemma 2. *Minimizing the contrastive loss \mathcal{L}_c is equivalent to maximizing the mutual information between generative representations \mathbf{f} and \mathbf{f}^+ , i.e., $E_c(G(\mathbf{z}, c))$ and $E_c(G(\mathbf{z}^+, c^+))$.*

$$\mathbb{E}_{\substack{(\mathbf{z}, c, \mathbf{z}^+, c^+) \sim p_{pos} \\ (\mathbf{z}_i, c_i^-) \stackrel{i.i.d.}{\sim} p(\mathbf{z}, neg(c))}} \left[-\log \frac{e^{(\mathbf{f}^T \mathbf{f}^+ / \tau)}}{e^{(\mathbf{f}^T \mathbf{f}^+ / \tau)} + \sum_i e^{(\mathbf{f}^T \mathbf{f}_i^- / \tau)}} \right] \geq \log(K) - I(\mathbf{f}, \mathbf{f}^+). \quad (\text{A.1})$$

Proof. Sample $(\mathbf{z}, c, \mathbf{z}^+, c^+)$ from p_{pos} to generate images $G(\mathbf{z}, c)$ and $G(\mathbf{z}^+, c^+)$, the representations \mathbf{f} and \mathbf{f}^+ are encoded by encoder E_c . We then sample $K - 1$ negative points (\mathbf{z}_i, c_i^-) to generate images $G(\mathbf{z}_i, c_i^-)$, and finally obtain $K - 1$ representations $\mathbf{f}_i^-, i = 1, \dots, K - 1$. \mathbf{f}^+ and $\{\mathbf{f}_i^-\}$ can construct a new set $\{\mathbf{f}_k\}_{k=1}^K$, where the k^{th} element is the representation generated from p_{pos} . The contrastive loss \mathcal{L}_c is the categorical cross-entropy of classifying the positive sample correctly. The optimal probability for this loss is:

$$p(d = k | \mathbf{f}, \{\mathbf{f}_i\}_{i=1}^{K-1}) = \frac{p(\mathbf{f}^+ | \mathbf{f}) \prod_{l \neq k} p(\mathbf{f}_l^-)}{\sum_{j=1}^N p(\mathbf{f}^+ | \mathbf{f}) \prod_{l \neq j} p(\mathbf{f}_l^-)} = \frac{p(\mathbf{f}^+ | \mathbf{f})}{p(\mathbf{f}^+)} = \frac{p(\mathbf{f}^+ | \mathbf{f})}{p(\mathbf{f}^+) + \sum_{j \neq k} \frac{p(\mathbf{f}_j^- | \mathbf{f})}{p(\mathbf{f}_j^-)}}, \quad (\text{A.2})$$

where $[d = k]$ is the indicator that the k^{th} sample is the 'positive' sample. Compare Eq. (A.1) and Eq. (A.2), we can obtain:

$$e^{(\mathbf{f}^d \mathbf{f}^+ / \tau)} \propto \frac{p(\mathbf{f}^+ | \mathbf{f})}{p(\mathbf{f}^+)}. \quad (\text{A.3})$$

Inserting this back to the contrastive loss \mathcal{L}_c :

$$\begin{aligned} \mathcal{L}_c^{\text{opt}} &= \mathbb{E}_{\substack{(\mathbf{z}, c, \mathbf{z}^+, c^+) \sim p_{\text{pos}} \\ (\mathbf{z}_i, c_i^-) \stackrel{i.i.d.}{\sim} p(\mathbf{z}, \text{neg}(c))}} \log \left[\frac{\frac{p(\mathbf{f}^+ | \mathbf{f})}{p(\mathbf{f}^+)}}{\frac{p(\mathbf{f}^+ | \mathbf{f})}{p(\mathbf{f}^+)} + \sum_i \frac{p(\mathbf{f}_i^- | \mathbf{f})}{p(\mathbf{f}_i^-)}} \right] \\ &= \mathbb{E}_{\substack{(\mathbf{z}, c, \mathbf{z}^+, c^+) \sim p_{\text{pos}} \\ (\mathbf{z}_i, c_i^-) \stackrel{i.i.d.}{\sim} p(\mathbf{z}, \text{neg}(c))}} \log \left[1 + \frac{p(\mathbf{f}^+)}{p(\mathbf{f}^+ | \mathbf{f})} \sum_i \frac{p(\mathbf{f}_i^- | \mathbf{f})}{p(\mathbf{f}_i^-)} \right] \end{aligned} \quad (\text{A.4})$$

$$\begin{aligned} &\approx \mathbb{E}_{(\mathbf{z}, c, \mathbf{z}^+, c^+) \sim p_{\text{pos}}} \log \left[1 + \frac{p(\mathbf{f}^+)}{p(\mathbf{f}^+ | \mathbf{f})} (K - 1) \right. \\ &\quad \left. \mathbb{E}_{(\mathbf{z}_i, c_i^-) \stackrel{i.i.d.}{\sim} p(\mathbf{z}, \text{neg}(c))} \frac{p(\mathbf{f}_i^- | \mathbf{f})}{p(\mathbf{f}_i^-)} \right] \end{aligned} \quad (\text{A.5})$$

$$= \mathbb{E}_{(\mathbf{z}, c, \mathbf{z}^+, c^+) \sim p_{\text{pos}}} \log \left[1 + \frac{p(\mathbf{f}^+)}{p(\mathbf{f}^+ | \mathbf{f})} (K - 1) \right] \quad (\text{A.6})$$

$$\geq \mathbb{E}_{(\mathbf{z}, c, \mathbf{z}^+, c^+) \sim p_{\text{pos}}} \log \left[\frac{p(\mathbf{f}^+)}{p(\mathbf{f}^+ | \mathbf{f})} K \right] \quad (\text{A.7})$$

$$= \log(K) - I(\mathbf{f}, \mathbf{f}^+) \quad (\text{A.8})$$

Minimizing the contrastive loss $\mathcal{L}_c(\mathbf{z}, c)$ is equivalent to maximizing the mutual information between \mathbf{f} and \mathbf{f}^+ . \square

Appendix B. Implementation Details

CoDeGAN comprises a generator G , a discriminator D , an encoder E_c , and an encoder E_z . Except on the CIFAR-10 dataset, the encoders E_c and E_z share weights except for the last layer. The value of τ was all set to be 0.07. The disentanglement accuracy, for MNIST, Fashion-MNIST, and CIFAR-10, is calculated following Mukherjee et al. (2019). That for COIL-20, 3D-Chairs, and 3D-Cars is calculated following the work (Ojha et al., 2020).

Appendix B.1. MNIST

On the MNIST dataset, the architecture of CoDeGAN followed the work (Mukherjee et al., 2019), which was based on WGAN-GP (Gulrajani et al., 2017). The batch size for the encoder, generator, and discriminator was 256, 64, and 64. The dimension of \mathbf{z} was 30, and c was encoded to be a one-hot vector. The dimensions of the representations \mathbf{f} and $\hat{\mathbf{z}}$ were set to be 120 and 30, respectively. β_1 and β_2 were set to be 75 and 0.0005.

Appendix B.2. Fashion-MNIST

On the Fashion-MNIST dataset, the architecture of CoDeGAN followed the work (Mukherjee et al., 2019), which was based on WGAN-GP (Gulrajani et al., 2017). The batch size was set to be 64 for G and D , 300 for E . The dimensions of \mathbf{f} , \mathbf{z} and $\hat{\mathbf{z}}$ were 120, 40 and 40, respectively. β_1 and β_2 were set to be 100 and 0.0005.

In pretraining, contrastive pretraining and meta pretraining are used to train E_c . Besides, the parameters of E_c were fixed in the first 200 epochs when training CoDeGAN. Some details are listed in the following:

- 1 In contrastive pretraining, SimCLR (Chen et al., 2020) was used to pretrain the encoder E_c for 200 epochs.
- 2 In meta pretraining, MAML (Finn et al., 2017) was used to pretrain the encoder E_c for 80 epochs, where supervised contrastive loss (Khosla et al., 2020) was used. The number of tasks was set to 10000, and each task included 5 ways. Both the support set and query set contained 20 shots, and 4 tasks were used in an iteration.

Appendix B.3. CIFAR-10

On the CIFAR-10 dataset, the network architecture of CoDeGAN followed SNGAN (Miyato et al., 2018), where the encoder's architecture was ResNet18 (He et al., 2016). The batch size for G , D , E_c , and E_z were 128, 64, 256, 32. The dimensions of \mathbf{f} , \mathbf{z} , and $\hat{\mathbf{z}}$ were set to be 128, 118, and 118, and c was encoded to be a 10-dimensional one-hot vector. In pretraining, contrastive pretraining and meta pretraining are used to train E_c . Besides, the parameters of E_c were fixed in the first 100 epochs when training CoDeGAN. Some details in pretraining are listed in the following:

- 1 In contrastive pretraining, SimCLR (Chen et al., 2020) was used to train E_c for 200 epochs.
- 2 In meta pretraining, MAML (Finn et al., 2017) was used to pretrain the encoder E_c for 40 epochs, where supervised contrastive loss (Khosla et al., 2020) was used. The Tiny-ImageNet dataset was chosen as the training set. The number of tasks was set to 10000, and each task included 10 ways. The support set contained 10 shots, the query set contained 20 shots, and 4 tasks were used in an iteration.

Appendix B.4. COIL-20

On the COIL-20 dataset, the network architecture of CoDeGAN followed WGAN-GP (Gulrajani et al., 2017) with BCE Loss. The batch size for G , D , E_c and E_z were 256, 128, 512, 64. The dimension of \mathbf{z} was 118, and c was encoded to be a 20-dimensional one-hot vector. The dimensions of the representations \mathbf{f} and $\hat{\mathbf{z}}$ were set to be 128 and 118, respectively. β_1 and β_2 were set to be 150 and 0.0005.

In contrastive pretraining, SimCLR (Chen et al., 2020), SimSiam (Chen and He, 2021) and NNCLR (Ermolov et al., 2021) were used to train E_c . Besides, the parameters of E_c were fixed in the first 1,500 epochs when training CoDeGAN. Some details

in pretraining are listed in the following: (i) SimCLR was used to pretrain the encoder E_c for 76 epochs. Adam optimizer was adopted with a learning rate of 0.0002 and betas (0.5, 0.99), β_1 was 100. The batch size is 256. (ii) SimSiam was used to pretrain the encoder E_c for 1,585 epochs, β_1 was 50. The other settings were the same as the SimCLR method. (iii) NNCLR was used to pretrain the encoder E_c for 209 epochs, β_1 was 50. The other settings were the same as the SimCLR method.

Appendix B.5. 3D-Chairs and 3D-Cars

On the 3D-Chairs and 3D-Cars datasets, the network architecture of CoDeGAN followed WGAN-GP (Gulrajani et al., 2017) with BCE Loss. The dimension of \mathbf{z} was 118. and c was encoded to be a 10-dimensional one-hot vector. The dimensions of the representations \mathbf{f} and $\hat{\mathbf{z}}$ were set be 128 and 118, respectively. β_1 and β_2 were set to be 100 and 0.0005.

In contrastive pretraining, for 3D-Chairs, the parameters of E_c were fixed in the first 1,000 epochs when training CoDeGAN, for 3D-Cars, the fixed epoch number and β_1 were 200 and 80. Some details in pretraining are listed in the following: (i) was used to pretrain the encoder E_c for 122 epochs. Adam optimizer was adopted with a learning rate of 0.0002 and betas (0.5, 0.99), β_1 was 75. The batch size is 256. (ii) SimSiam was used pretrain the encoder E_c for 989 epochs. The other settings were the same as the SimCLR method. (iii) NNCLR was used pretrain the encoder E_c for 405 epochs, β_1 was 50. The other settings were the same as the SimCLR method.

Appendix C. More Results

Appendix C.1. Robustness to Intra-class Variations

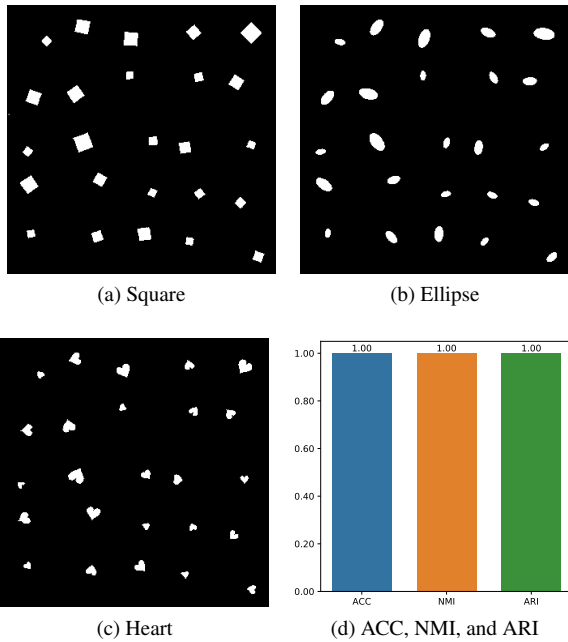


Figure C.10: **Images generated by CoDeGAN trained on dSprites.** (a), (b), and (c) show the images corresponding to the three shapes, respectively. CoDeGAN is robust to intra-class changes, such as scale, rotation, and translation.

To test the robustness of CoDeGAN to intra-class variations, we conduct experiments on the dSprites dataset (Matthey et al., 2017). The dSprites dataset consists of 737,280 binary 64×64 images of 2D shapes. On the dSprites dataset, the network architecture of CoDeGAN followed SNGAN (Lin et al., 2020), and the encoder’s architecture followed the Q-network of InfoGAN-CR (Lin et al., 2020). The GAN’s loss was the traditional JSD loss as in InfoGAN-CR (Lin et al., 2020). The batch size was set to 150 for the generator, 300 for the discriminator, and the encoder. The dimensions of \mathbf{f} , \mathbf{z} , and $\hat{\mathbf{z}}$ were 40, 52 and 52. In addition, $\beta_1 = 1$, and $\beta_2 = 0.0001$. E_c was pretrained by SimCLR for 100 epochs and further fine-tuned for 20 epochs using few labeled images. The parameters of E_c were fixed in the first 100 epochs, and CoDeGAN was trained for 300 epochs. 727,280 images were used for training, and the rest 10,000 for testing. 0.21% of the training samples were set to have labels.

It has five independent latent factors: shape, scale, rotation, x , and y positions of a sprite. The shape contains three categories: square, ellipse, and heart. Fig. C.10 shows the disentangled results on dSprites dataset. Figs. C.10a to C.10c show the generation results of changing factor c and \mathbf{z} , where the shape “square”, “ellipse”, and “heart” are generated orderly. These results reveal our CoDeGAN with few labels is robust to intra-class changes, such as scale, rotation, and translation. This should own to our loss function, which, coupled with contrastive prior, can utilize few labels to the largest extent. The ACC, NMI, and ARI are all close to 1, even though only 0.21% of labels are involved.

Appendix C.2. Sensitivity to Tiny Inter-Class Variation

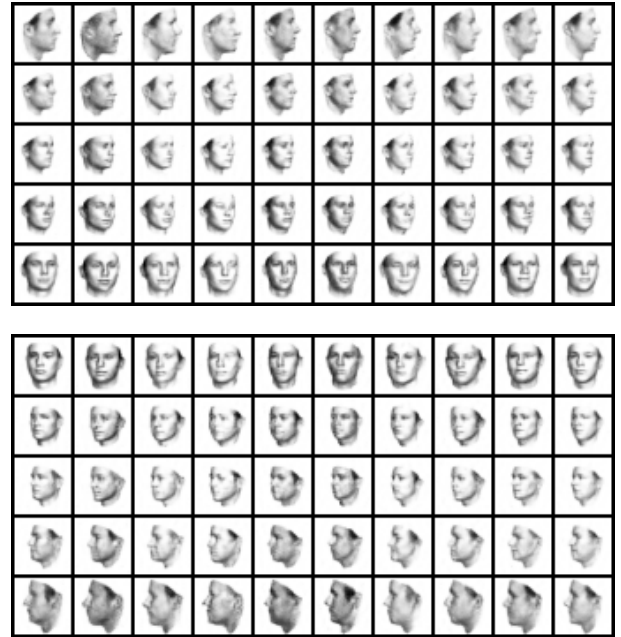


Figure C.11: **Images generated by CoDeGAN trained on Faces.** Each row corresponds to one latent factor value. Experiments show CoDeGAN has the potential to disentangle class with a tiny variation.

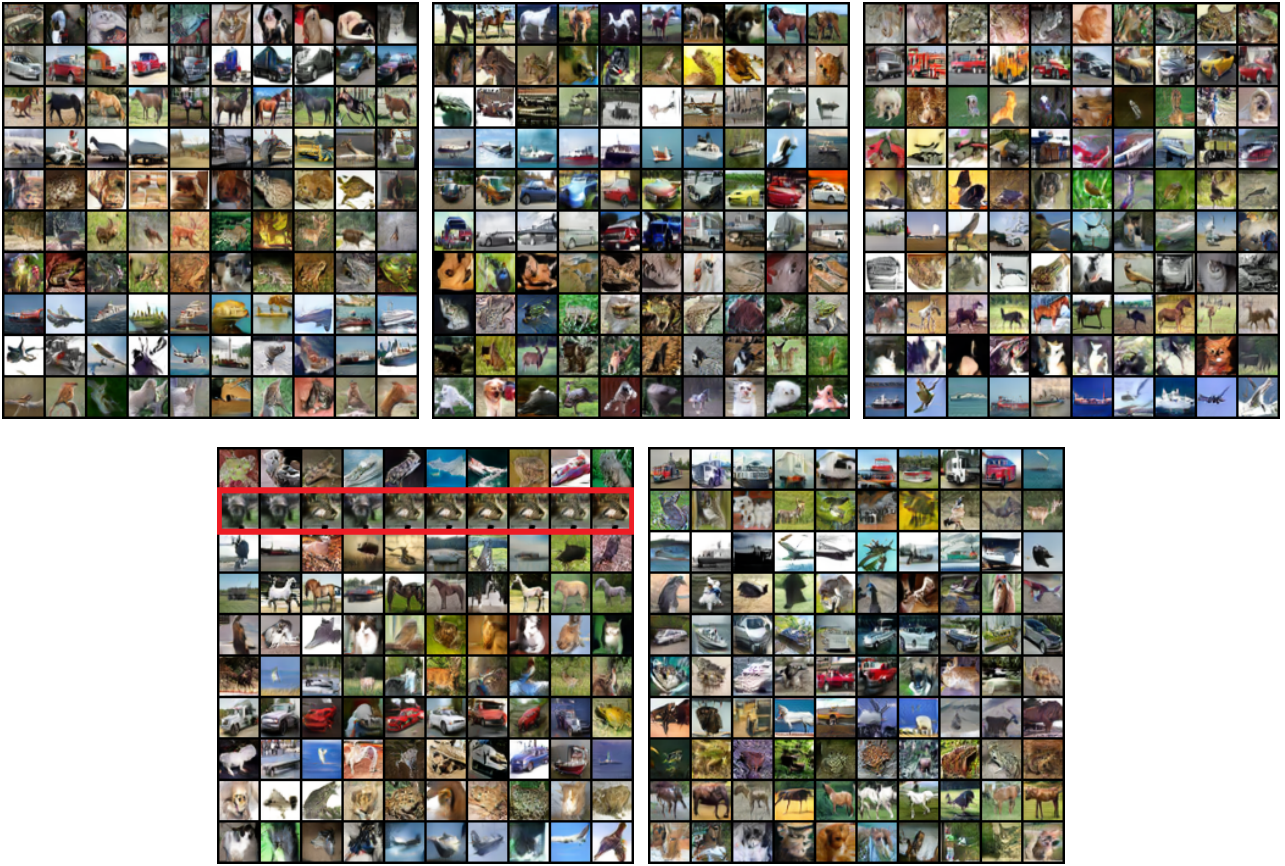


Figure C.12: **5 Times Generation Results for CIFAR-10 with L_c on the layers $L_2 + L_3 + L_4$.** Red box highlights mode collapse/dropping.

To test the sensitivity of CoDeGAN to tiny inter-class variation, we conduct experiments on the Faces datasets (Paysan et al., 2009). The Faces dataset contains variation factors such as azimuth (pose), elevation, and lighting. On the Faces dataset, the network architecture of CoDeGAN followed InfoGAN (Chen et al., 2016), but without batch normalization in the discriminator. The encoder’s architecture was the same as the discriminator except for the last layer. The GAN’s loss followed the WGAN-GP (Gulrajani et al., 2017). The batch size for the generator and the discriminator was set to 300, and that for the encoder was 1500. The dimension of \mathbf{f} , \mathbf{z} and $\hat{\mathbf{z}}$ was 118. Besides, $\beta_1 = 10$, and $\beta_2 = 10$. We trained CoDeGAN for 600 epochs on the Faces dataset. 1% of the training samples were with labels. E_c was pretrained by SimCLR for 200 epochs and further fine-tuned for 20 epochs using few labeled images. When training CoDeGAN, the parameters of E_c were fixed in the first 200 epochs.

To build a training set, 10,000 face prototypes were synthesized, and ten face images were generated for each face prototype with a pose from -90° to $+90^\circ$. Fig. C.11 shows the disentangled results on the Faces dataset, where each row corresponds to a different head pose. We discretized the continuous pose change to discrete pose change; the interval between each group is 20° . We observe in Fig. C.11, compared with digits, objects, or shapes, the images in adjacent categories are very

similar. This demonstrates CoDeGAN also has the potential to disentangle class with a tiny variation.

Appendix C.3. Ablation Study

We study the effects of contrastive loss on different feature layers. The features from four layers of the encoder network E_c at different resolutions ($L_1 = 32^2, L_2 = 16^2, L_3 = 8^2, L_4 = 4^2$) were extracted. Here, L_4 denotes the highest feature layer, and L_1 denotes the lowest feature layer, which is most *close* to the generated image. The features were down-sampled four times as well as flattened. Then, the multi-scale features were fed to a two-layer MLP and reduced to the same 128 dimensions.

We show generated images with L_c on different feature layers for CIFAR-10, as shown in Figs. C.12 and C.13. Mode collapse/dropping sometimes occurs when adding contrastive loss on lower feature layers. This tendency may be explained by the fact that the similarity constraints relaxing on low-layer features are minimal. This is because these layers are close to the image, and the model capacity of the low-layer sub-networks of encoder E_c is restricted.

References

- Arora, S., Khandeparkar, H., Khodak, M., Plevrakis, O., Saunshi, N., 2019. A theoretical analysis of contrastive unsupervised representation learning. arXiv preprint arXiv:1902.09229 .



Figure C.13: 5 Times Generation Results for CIFAR-10 with L_c on all layers $L_1 + L_2 + L_3 + L_4$. Red box highlights mode collapse/dropping.

- Aubry, M., Maturana, D., Efros, A.A., Russell, B.C., Sivic, J., 2014. Seeing 3D chairs: exemplar part-based 2D-3D alignment using a large dataset of CAD models, in: CVPR, pp. 3762–3769.
- Benny, Y., Wolf, L., 2020. OneGAN: Simultaneous unsupervised learning of conditional image generation, foreground segmentation, and fine-grained clustering, in: ECCV, Springer, pp. 514–530.
- Caron, M., Misra, I., Mairal, J., Goyal, P., Bojanowski, P., Joulin, A., 2020. Unsupervised learning of visual features by contrasting cluster assignments. *NeurIPS* 33, 9912–9924.
- Caron, M., Touvron, H., Misra, I., Jégou, H., Mairal, J., Bojanowski, P., Joulin, A., 2021. Emerging properties in self-supervised vision transformers, in: ICCV, pp. 9650–9660.
- Chen, T., Kornblith, S., Norouzi, M., Hinton, G., 2020. A simple framework for contrastive learning of visual representations, in: ICML, PMLR, pp. 1597–1607.
- Chen, T.Q., Li, X., Grosse, R.B., Duvenaud, D., 2018. Isolating sources of disentanglement in variational autoencoders., in: ICLR.
- Chen, X., Duan, Y., Houthoofd, R., Schulman, J., Sutskever, I., Abbeel, P., 2016. InfoGAN: Interpretable representation learning by information maximizing generative adversarial nets, in: *NeurIPS*, pp. 2180–2188.
- Chen, X., He, K., 2021. Exploring simple siamese representation learning, in: CVPR, pp. 15750–15758.
- Doshi-Velez, F., Kim, B., 2017. Towards a rigorous science of interpretable machine learning. *arXiv preprint arXiv:1702.08608*.
- Dwivedi, D., Aytar, Y., Tompson, J., Sermanet, P., Zisserman, A., 2021. With a little help from my friends: Nearest-neighbor contrastive learning of visual representations, in: ICCV, pp. 9588–9597.
- Ermolov, A., Siarohin, A., Sangineto, E., Sebe, N., 2021. Whitening for self-supervised representation learning, in: ICML, PMLR, pp. 3015–3024.
- Esser, P., Rombach, R., Ommer, B., 2020. A disentangling invertible interpretation network for explaining latent representations, in: CVPR, pp. 9223–9232.
- Fidler, S., Dickinson, S., Urtasun, R., 2012. 3D object detection and viewpoint estimation with a deformable 3D cuboid model, in: *NeurIPS*, p. 611–619.
- Finn, C., Abbeel, P., Levine, S., 2017. Model-agnostic meta-learning for fast adaptation of deep networks, in: ICML, pp. 1126–1135.
- Gabbay, A., Hoshen, Y., 2020. Demystifying inter-class disentanglement, in: ICLR.
- Gulrajani, I., Ahmed, F., Arjovsky, M., Dumoulin, V., Courville, A.C., 2017. Improved training of Wasserstein GANs, in: *NeurIPS*, pp. 5767–5777.
- Härkönen, E., Hertzmann, A., Lehtinen, J., Paris, S., 2020. GANSpace: Discovering interpretable GAN controls. *NeurIPS* 33, 9841–9850.
- He, K., Chen, X., Xie, S., Li, Y., Dollár, P., Girshick, R., 2022. Masked autoencoders are scalable vision learners, in: CVPR, pp. 16000–16009.
- He, K., Fan, H., Wu, Y., Xie, S., Girshick, R., 2020. Momentum contrast for unsupervised visual representation learning, in: CVPR, pp. 9729–9738.
- He, K., Zhang, X., Ren, S., Sun, J., 2016. Deep residual learning for image recognition, in: CVPR, pp. 770–778.
- Heusel, M., Ramsauer, H., Unterthiner, T., Nessler, B., Hochreiter, S., 2017. GANs trained by a two time-scale update rule converge to a local nash equilibrium, in: *NeurIPS*, pp. 6626–6637.
- Higgins, I., Matthey, L., Pal, A., Burgess, C., Glorot, X., Botvinick, M., Mohamed, S., Lerchner, A., 2016. beta-VAE: Learning basic visual concepts with a constrained variational framework, in: ICLR.
- Hjelm, R.D., Fedorov, A., Lavoie-Marchildon, S., Grewal, K., Bachman, P., Trischler, A., Bengio, Y., 2018. Learning deep representations by mutual information estimation and maximization. *arXiv preprint arXiv:1808.06670*.
- Hwang, U., Kim, H., Jung, D., Jang, H., Lee, H., Yoon, S., 2021. Stein latent optimization for generative adversarial networks, in: ICLR.
- Jaiswal, A., Babu, A.R., Zadeh, M.Z., Banerjee, D., Makedon, F., 2021. A survey on contrastive self-supervised learning. *Technologies* 9, 2.
- Kappiyath, A., Sreelatha, S.V., Sumitra, S., 2022. Self-supervised enhancement of latent discovery in GANs, in: AAAI, pp. 7078–7086.

- Karras, T., Laine, S., Aila, T., 2019. A style-based generator architecture for generative adversarial networks, in: CVPR, pp. 4401–4410.
- Khosla, P., Teterwak, P., Wang, C., Sarna, A., Tian, Y., Isola, P., Maschinot, A., Liu, C., Krishnan, D., 2020. Supervised contrastive learning. arXiv preprint arXiv:2004.11362 .
- Kim, H., Mnih, A., 2018. Disentangling by factorising, in: ICML, pp. 2649–2658.
- Kim, Y., Ha, J.W., 2021. Contrastive fine-grained class clustering via generative adversarial networks, in: ICLR.
- Kingma, D.P., Welling, M., 2014. Auto-encoding variational bayes, in: ICLR.
- Krizhevsky, A., Hinton, G., et al., 2009. Learning multiple layers of features from tiny images. Master’s thesis, Department of Computer Science, University of Toronto .
- Lakkaraju, H., Bach, S.H., Leskovec, J., 2016. Interpretable decision sets: A joint framework for description and prediction, in: Proceedings of the 22nd ACM SIGKDD International Conference on Knowledge Discovery and Data Mining, pp. 1675–1684.
- Lecun, Y., Bottou, L., Bengio, Y., Haffner, P., 2001. Gradient-based learning applied to document recognition. *Intelligent Signal Processing* , 306–351.
- Li, J., Li, D., Xiong, C., Hoi, S., 2022. BLIP: Bootstrapping language-image pre-training for unified vision-language understanding and generation, in: ICML, PMLR, pp. 12888–12900.
- Li, Y., Singh, K.K., Ojha, U., Lee, Y.J., 2020. MixNMatch: Multifactor disentanglement and encoding for conditional image generation, in: CVPR, pp. 8039–8048.
- Lin, Z., Thekumparampil, K., Fanti, G., Oh, S., 2020. InfoGAN-CR: Disentangling generative adversarial networks with contrastive regularizers, in: ICML.
- Liu, B., Zhu, Y., Fu, Z., de Melo, G., Elgammal, A., 2020. OOGAN: Disentangling GAN with one-hot sampling and orthogonal regularization, in: AAAI, pp. 4836–4843.
- Locatello, F., Tschannen, M., Bauer, S., Ratsch, G., Scholkopf, B., Bachem, O., 2020. Disentangling factors of variations using few labels, in: ICLR.
- Matthey, L., Higgins, I., Hassabis, D., Lerchner, A., 2017. DSprites: Disentanglement testing sprites dataset. <https://github.com/deepmind/dsprites-dataset/>.
- Miyato, T., Kataoka, T., Koyama, M., Yoshida, Y., 2018. Spectral normalization for generative adversarial networks. arXiv preprint arXiv:1802.05957 .
- Mohamed, S., Lakshminarayanan, B., 2016. Learning in implicit generative models. arXiv preprint arXiv:1610.03483 .
- Mukherjee, S., Asnani, H., Lin, E., Kannan, S., 2019. ClusterGAN: Latent space clustering in generative adversarial networks, in: AAAI, pp. 4610–4617.
- Nene, S.A., Nayar, S.K., Murase, H., 1996. Columbia object image library (COIL-20). Technical Report .
- Ojha, U., Singh, K.K., Hsieh, C.J., Lee, Y.J., 2020. Elastic-InfoGAN: Unsupervised disentangled representation learning in class-imbalanced data, in: NeurIPS, pp. 18063–18075.
- Oord, A.v.d., Li, Y., Vinyals, O., 2018. Representation learning with contrastive predictive coding. arXiv preprint arXiv:1807.03748 .
- Pan, L., Cheng, S., Liu, J., Tang, P., Wang, B., Ren, Y., Xu, Z., 2020. Latent Dirichlet allocation based generative adversarial networks. *Neural Networks* 132, 461–476.
- Paysan, P., Knothe, R., Amberg, B., Romdhani, S., Vetter, T., 2009. A 3D face model for pose and illumination invariant face recognition, in: 2009 Sixth IEEE International Conference on Advanced Video and Signal Based Surveillance, pp. 296–301. doi:10.1109/AVSS.2009.58.
- Radford, A., Kim, J.W., Hallacy, C., Ramesh, A., Goh, G., Agarwal, S., Sastry, G., Askell, A., Mishkin, P., Clark, J., et al., 2021. Learning transferable visual models from natural language supervision, in: ICML, PMLR, pp. 8748–8763.
- Ren, X., Yang, T., Wang, Y., Zeng, W., 2021. Learning disentangled representation by exploiting pretrained generative models: A contrastive learning view. arXiv preprint arXiv:2102.10543 .
- Rudin, C., 2019. Stop explaining black box machine learning models for high stakes decisions and use interpretable models instead. *Nature Machine Intelligence* 1, 206–215.
- Salimans, T., Goodfellow, I., Zaremba, W., Cheung, V., Radford, A., Chen, X., 2016. Improved techniques for training GANs, in: NeurIPS, pp. 2234–2242.
- Shen, Y., Gu, J., Tang, X., Zhou, B., 2020. Interpreting the latent space of gans for semantic face editing, in: CVPR, pp. 9243–9252.
- Shen, Y., Zhou, B., 2021. Closed-form factorization of latent semantics in GANs, in: CVPR, pp. 1532–1540.
- Shu, R., Chen, Y., Kumar, A., Ermon, S., Poole, B., 2020. Weakly supervised disentanglement with guarantees, in: ICLR.
- Sohn, K., 2016. Improved deep metric learning with multi-class n-pair loss objective, in: NeurIPS, pp. 1857–1865.
- Tschannen, M., Djolonga, J., Rubenstein, P.K., Gelly, S., Lucic, M., 2019. On mutual information maximization for representation learning. arXiv preprint arXiv:1907.13625 .
- Wang, T., Isola, P., 2020. Understanding contrastive representation learning through alignment and uniformity on the hypersphere, in: ICML, pp. 9929–9939.
- Wang, X., Zhang, R., Shen, C., Kong, T., Li, L., 2021. Dense contrastive learning for self-supervised visual pre-training, in: CVPR, pp. 3024–3033.
- Wu, M., Zhuang, C., Mosse, M., Yamins, D., Goodman, N., 2020. On mutual information in contrastive learning for visual representations. arXiv preprint arXiv:2005.13149 .
- Wu, Z., Xiong, Y., Yu, S.X., Lin, D., 2018. Unsupervised feature learning via non-parametric instance discrimination, in: CVPR, pp. 3733–3742.
- Xiao, H., Rasul, K., Vollgraf, R., 2017. Fashion-MNIST: A novel image dataset for benchmarking machine learning algorithms. arXiv preprint arXiv:1708.07747 .
- Zhang, Q., Wu, Y.N., Zhu, S.C., 2018. Interpretable convolutional neural networks, in: CVPR, pp. 8827–8836.